JOURNAL OF GEOPHYSICAL RESEARCH, VOL. 103, NO. C10, PAGES 21,481–21,497, SEPTEMBER 15, 1998

Lateral mixing and the North Atlantic Tracer Release Experiment: Observations and numerical simulations of Lagrangian particles and a passive tracer

Miles A. Sundermeyer[1]

Joint Program in Physical Oceanography, Massachusetts Institute of Technology and Woods Hole Oceanographic Institution, Woods Hole, Massachusetts

James F. Price

Department of Physical Oceanography, Woods Hole Oceanographic Institution, Woods Hole, Massachusetts

Abstract. Mixing and stirring of Lagrangian particles and a passive tracer were studied by comparison of float and tracer observations from the North Atlantic Tracer Release Experiment (NATRE). Statistics computed from the NATRE floats were found to be similar to those estimated by *Ledwell et al.* [this issue] from the tracer dispersion. Mean velocities computed from the floats were $(\overline{u}, \overline{v}) = (-1.2 \pm 0.3,\ -0.9 \pm 0.2)$ cm/s for the (zonal, meridional) components, and large-scale effective eddy diffusivities were $(\kappa_{e11}, \kappa_{e22}) = (1.5 \pm 0.7,\ 0.7 \pm 0.4) \times 10^3$ m^2/s. The NATRE observations were used to evaluate theoretical models of tracer and particle dispersal. The tracer dispersion observed by *Ledwell et al.* [this issue] was consistent with an exponential growth phase for about the first 6 months and a linear growth at larger times. A numerical model of mesoscale turbulence that was calibrated with float statistics also showed an exponential growth phase of tracer and a reduced growth for longer times. Numerical results further show that *Garrett*'s [1983] theory, relating the effective small-scale diffusivity to the rms strain rate and tracer streak width, requires a scale factor of 2 when the observed growth rate of streak length is used as a measure of the strain rate. This scale factor will be different for different measures of the strain rate and may also be affected by temporal and spatial variations in the mesoscale strain field.

1. Introduction

The kinematics of tracer dispersal provides a basis for describing the distribution of natural and anthropogenic tracers in the ocean. In this paper we examine the horizontal dispersion of a localized tracer observed during the North Atlantic Tracer Release Experiment (NATRE). Our goal is to understand what these observations can tell us about both small- and large-scale advective and diffusive processes in the ocean.

1.1. Stirring and Mixing in a Turbulent Ocean

To begin, it is helpful to imagine that tracer dispersal is a combination of two different types of processes: "mixing" processes, which act to reduce tracer gradients, and "stirring" processes, which act to increase tracer gradients [*Eckart*, 1948]. Put another way, mixing processes are those which can (or must) be modeled by diffusion, i.e., molecular or very small-scale advective processes in which individual exchange events are not resolved, while stirring processes are resolved events, e.g., the streaking and folding of a tracer within a resolved eddy field. The distinction between these two types of processes is, in practice, one of small versus large scale or, in a modeling context, subgrid-scale parameterized motions versus resolved motions.

Classical theory can predict the rate of tracer dispersal in the presence of a purely diffusive and very simple advective process [e.g., *Fischer et al.*, 1979]. However, when shearing and straining occur on different scales, as in a turbulent ocean, the analysis is far more complex and models must be built with uncertain approximations.

Consider the fate of a localized release of a passive tracer into a turbulent ocean. A useful simplification, suggested by *Garrett* [1983], is to model the dispersal of tracer in three distinct stages. During the first stage, while the scale of the tracer patch is much smaller than

[1]Now at the Center for Marine Science and Technology, University of Massachusetts, New Bedford.

Paper number 98JC01999.
0148-0227/98/98JC-01999$09.00

that of the straining eddies, the patch growth can be modeled as a mixing or diffusive process. For such times, assuming a patch radius of 2σ, where σ^2 is the patch variance, the area A occupied by the tracer will grow linearly in time,

$$A = 8\pi\kappa_s t, \tag{1}$$

where κ_s is an effective small-scale diffusivity and t is time. *Young et al.* [1982] predicted that the magnitude of this small-scale diffusivity is of order $\kappa_s \sim (N^2/f^2)\kappa_z$, where N is the buoyancy frequency, f is the Coriolis parameter, and κ_z is the vertical diffusivity. For the NATRE region, *Ledwell et al.* [this issue] found that this prediction yields $\kappa_s \approx 0.08$ m^2/s, and was consistent with the initial dispersion of their tracer injection streaks.

As the size of the patch grows, it will eventually reach a size where the mesoscale strain field begins to advect the tracer into long, thin streaks. (For a point release, this will occur after time $t \sim 1/2\gamma_{\rm rms}$, where $\gamma_{\rm rms}$ is the rms mesoscale strain rate.) The rate of dispersal may then accelerate to a second stage in which the streak length L grows exponentially in time, $L = L_o e^{\lambda t}$, where $L_o = 2(\kappa_s/\gamma_{\rm rms})^{1/2}$ is the transition scale of the patch. *Garrett* [1983] presumed that the streak growth rate λ should be nearly equal to the rms strain rate; that is, $\lambda = \alpha\gamma_{\rm rms}$, where α is an order 1 coefficient to be determined. Meanwhile, the width of the streaks is presumed to be set by a balance between the narrowing tendency of the convergent strain field and the small-scale diffusion or mixing, which acts to widen the streak; that is, $\sigma^2_{\rm rms} = \kappa_s/\gamma_{\rm rms}$, where $\sigma^2_{\rm rms}$ is the rms cross-streak variance. (Given observations from a tracer release experiment such as NATRE, $\gamma_{\rm rms}$ cannot be measured directly and must be inferred from the streak growth rate, which is the only accessible measure of strain.) During the second stage of dispersal, on the basis of this combination of along- and cross-streak dynamics, the tracer area is expected to grow exponentially in time,

$$A = 4\pi(\kappa_s/\gamma_{\rm rms})e^{[\alpha\gamma_{\rm rms}(t-\frac{1}{2}\gamma_{\rm rms}^{-1})]} \tag{2}$$

(this follows *Garrett* [1983, equation (2.3)], except for the leading factor of 4 in our result and a factor of 1/2 in the exponent rather than 1/4, which arise from different definitions of length and timescales).

Exponential growth will continue until the horizontal scale of the tracer patch exceeds that of the mesoscale eddies. At that time, the tracer dispersal enters a third stage in which continued stirring by the eddies causes streaks to wrap around one another, eventually making the patch more homogeneous. Subsequently, for times much longer than the Lagrangian integral timescale (about 10 days; see below for definition), the rate of dispersal of the patch as a whole may again be modeled as a diffusive process, with area increasing linearly in time,

$$A = 8\pi\kappa_e t, \tag{3}$$

where κ_e is the effective eddy diffusivity due to the mesoscale eddies and is typically of order $\kappa_e \sim 10^3$ m^2/s.

This framework has proven useful for describing tracer dispersal in numerical models. For example, simulations by *Haidvogel and Keffer* [1984] showed rapid development of tracer streaks that were consistent with an exponential growth (see section 5 for further discussion of their definition of the rms strain rate). Their simulations also showed an initial increase in small-scale tracer variance, possibly corresponding to the initial sharpening of tracer gradients by the mesoscale strain, followed by a slow smooth decay, consistent with the expected transition to diffusive spreading for large times. The evolution of a continuous tracer with a large-scale concentration gradient has been studied by *Holloway and Kristmannsson* [1984], who showed that an effective eddy diffusivity formulation can also be used in that case and that such a diffusivity agrees with simple mixing length arguments. The idea of an effective eddy diffusivity is also supported by numerous observational studies of Lagrangian particle dynamics [e.g., *Freeland et al.*, 1975; *Colin de Verdiere*, 1983; *Davis*, 1985]. The relationship between Lagrangian particle and passive tracer has also been discussed, for example, by *Davis* [1983, 1987] and *Bennett* [1987]. These studies have furthered our understanding of how tracer and particle dispersal would be influenced by turbulent stirring; however, until recently, there had been little opportunity to compare them directly with oceanic observations of a localized release of passive tracer.

1.2. Goals and Outline

The 1992 North Atlantic Tracer Release Experiment provided unique observations of the dispersal of a passive tracer and Lagrangian particles in open-ocean conditions. A thorough description of the lateral dispersion characteristics of the tracer was provided by *Ledwell et al.* [this issue]. In the present work, we examine particle statistics computed from the NATRE float data and use both the tracer and float data in conjunction with a numerical model to study lateral mixing and stirring in the open ocean. We address he following three questions:

1. How do the statistics computed from the NATRE float data compare with similar statistics computed from the NATRE tracer data?
2. Is *Garrett*'s [1983] model of a three-stage tracer dispersal qualitatively consistent with the observed dispersion rates estimated from the NATRE field experiment?
3. What are the biases and uncertainties associated with using *Garrett*'s [1983] model to make quantitative estimates of the strain rate, streak width, and small-scale diffusivity?

In section 2, we introduce some statistical tools for quantifying the dispersal and diffusion of Lagrangian

particles and passive tracer. Section 3 provides an overview of the NATRE experiment and the tracer results, along with a statistical description of the float dispersal. Also in section 3, we address questions 1 and 2 by examining the observations in the context of the initial streakiness of a passive tracer and the concept of effective eddy diffusivity for long times [*Garrett*, 1983; *Taylor*, 1921]. In section 4, we introduce a numerical model that is used to simulate tracer and float dispersal. We show that the simulated tracer behavior is qualitatively consistent with the theoretical model of *Garrett* [1983]. Question 3 is then addressed using our numerical results as a quantitative test of *Garrett*'s [1983] scaling arguments. In section 5, we offer a discussion of the possible biases and uncertainties associated with applying this scaling to a temporally and spatially varying strain field. Finally, in section 6, we summarize our results and their implications for the NATRE field study.

2. Theoretical Background

2.1. Formation of Tracer Streaks

In the present study, we are particularly interested in the second and third stages of dispersal, when the tracer is under the influence of the mesoscale strain field. Consider a patch made up of fully developed tracer streaks that have not yet begun to merge. During this second stage of dispersal, *Garrett* [1983] suggested that the mean streak width is set by a balance between the strain rate and small-scale diffusivity and that the growth of the area of the tracer patch should scale as the product of the along-streak growth rate times the mean streak width. For the purpose of quantitative diagnosis, e.g., using observed streak length and width to estimate strain rate and small-scale diffusivity [*Ledwell et al.*, 1993, this issue], we now examine an exact solution to the advection/diffusion equation and consider the effects of time dependence on this result.

Consider the case of a two-dimensional linear strain field in which the strain rate, $\gamma = \partial u/\partial x = -\partial v/\partial y$, is allowed to vary in time, but not in space (spatial dependence and eddy diffusivity are discussed in section 2.2). Furthermore, assume that small-scale dispersion processes can be parameterized in terms of an effective diffusivity κ_s. In this case, the concentration of tracer θ can be described by the familiar advection/diffusion equation,

$$\frac{\partial\theta}{\partial t} + \gamma x\frac{\partial\theta}{\partial x} - \gamma y\frac{\partial\theta}{\partial y} = \kappa_s\nabla^2\theta. \tag{4}$$

If we assume an initial condition for θ that is Gaussian in x and y (as might result from a purely diffusive process at scales small compared to the strain field), the concentration as a function of space and time can be expressed as

$$\theta = \theta_m(t)e^{-[(x^2/2\sigma_x^2)+(y^2/2\sigma_y^2)]}, \tag{5}$$

where the along- and cross-streak variances, σ_x^2 and σ_y^2, are governed by

$$\frac{d\sigma_x^2}{dt} - 2\gamma\sigma_x^2 = 2\kappa_s, \tag{6}$$

$$\frac{d\sigma_y^2}{dt} + 2\gamma\sigma_y^2 = 2\kappa_s, \tag{7}$$

respectively. $\theta_m = M/\sigma_x\sigma_y$ is the peak concentration, with M equal to the total mass of tracer, and $\gamma > 0$ is assumed (this analysis is similar to that of *Townsend* [1951]).

For a small initial patch, $\sigma_x^2, \sigma_y^2 \ll \kappa_s/\gamma$, and for small times, the effects of the strain are negligible and (6) and (7) reduce to the diffusive limit that characterizes stage 1. For longer times when the strain is important, a temporal average of (7) shows that the cross-streak variance satisfies

$$\langle\gamma\sigma_y^2\rangle = \langle\gamma\rangle\langle\sigma_y^2\rangle + \langle\gamma'\sigma_y^{2\prime}\rangle = \kappa_s, \tag{8}$$

where primed variables represent fluctuations about the mean values and we have assumed $\langle d\sigma_y^2/dt\rangle = 0$, which may apply following a tracer parcel in a stationary turbulent flow. Meanwhile, in the along-streak direction, (6) is satisfied by the general solution

$$\sigma_x^2 = \sigma_{xo}^2 e^{2\Gamma} + e^{2\Gamma}\int_0^t 2\kappa_s e^{-2\Gamma}dt, \tag{9}$$

with the exponential growth rate $\Gamma = \int_0^{t'}\gamma(t)dt$. If we identify $4\sigma_y$ as the streak width and $4\sigma_x$ as the streak length, in the limiting case of steady γ, (8) and (9) are similar to *Garrett*'s [1983; equation (2.3)] for the second stage of dispersal.

There are two points to be made regarding this solution. First, even after neglecting spatial dependence of the strain rate, (8) suggests that the strain rate and the streak width may hold a more subtle relationship than scaling arguments alone can reveal. For example, in this case, there is a covariance term generated by the product of γ and σ_y^2. Second, if we intend to use *Garrett*'s [1983] results for quantitative purposes, then we must define an appropriate measure of the strain rate and streak width for tracer in a fully turbulent flow. These two points lie near the heart of this study and are discussed in some detail in section 5.

2.2. Particle Dispersal and Effective Eddy Diffusivity

During the third stage of tracer dispersal, the concept of effective eddy diffusivity can be applied based on statistical considerations of particle dispersal in a turbulent flow [*Taylor*, 1921]. We now define a number of statistical quantities that are useful in later sections to characterize the large-scale flow field. In what follows, we assume an unbounded ocean that is horizontally homogeneous and statistically stationary over the

scales of interest. This ocean has been seeded with a large number of Lagrangian particles or neutrally buoyant floats.

Given such an ensemble of Lagrangian particles, a measure of the spatial and temporal scales of the flow can be obtained from the spatial correlation functions (SCFs) and Lagrangian autocorrelation functions (LACFs), respectively. The isotropic SCFs, $S_{ii}(\xi)$, are defined as

$$S_{ii}(\xi) = \frac{\langle v_i'(d)v_i'(d+\xi)\rangle}{\overline{\langle v_i'^2\rangle}}, \tag{10}$$

where ξ is the separation distance from an arbitrary position d and v_i' $(i = 1, 2)$ represent the transverse and longitudinal components of velocity, respectively. The double subscripts $ii = (11, 22)$ denote (transverse, longitudinal) spatial correlation functions. Angled brackets denote averages for an ensemble of Lagrangian particles, while the overbar denotes a temporal average.

The LACFs, $R_{ii}(\tau)$, are defined as

$$R_{ii}(\tau) = \frac{\langle u_i'(t)u_i'(t+\tau)\rangle}{\overline{\langle u_i'^2\rangle}}, \tag{11}$$

where τ is the time lag from an arbitrary time t and u_i' $(i = 1, 2)$ now represent zonal and meridional components of the Lagrangian velocity. The double subscripts $ii = (11, 22)$ denote (zonal, meridional) autocorrelation functions. The characteristic or integral timescale is defined as

$$I_{ii} = \int_0^\infty R_{ii}(\tau)d\tau, \tag{12}$$

provided this integral converges (for isotropic turbulence, $I_{11} = I_{22}$).

Taylor [1921] showed how to estimate large-scale stirring from Lagrangian observations. Given the assumptions above and assuming the motion has zero mean, the mean square particle displacement, i.e., the dispersion, is related to the eddy kinetic energy through the exact relation

$$\langle x_i'^2(t)\rangle = 2\overline{\langle u_i'^2\rangle}\int_0^t\int_0^T R_{ii}(\tau)d\tau dT. \tag{13}$$

In what follows, the mean eddy kinetic energy (EKE) is defined as

$$\frac{1}{2}\overline{\langle u_i'^2\rangle} = \frac{1}{2}\overline{\langle u_1'^2 + u_2'^2\rangle}.$$

If τ is small, R_{ii} does not differ appreciably from unity and (13) simplifies to

$$\langle x_i'^2(t)\rangle = \overline{\langle u_i'^2\rangle}\, t^2, \tag{14}$$

which says that the dispersion is proportional to the time since release squared and the eddy kinetic energy. For long times, R_{ii} should approach zero in a turbulent flow, so that the first integral in (13) becomes saturated,

$$\int_0^T R_{ii}(\tau)d\tau = I_{ii} = \text{const}, \tag{15}$$

and (13) reduces to

$$\langle x_i'^2(t)\rangle = 2\overline{\langle u_i'^2\rangle}I_{ii}t = 2\kappa_{e_{ii}}t. \tag{16}$$

Thus, for long times, particles disperse at a constant rate that is proportional to the mean square eddy velocity and the integral timescale of the turbulence. This constant rate of dispersion, $\kappa_{e_{ii}} = \overline{\langle u_i'^2\rangle}I_{ii}$, defines the effective eddy diffusivity of a stationary homogeneous turbulent flow and corresponds to stage 3 of *Garrett*'s [1983] model. (The limit of small τ in Taylor's single-particle theory has no direct analog in Garrett's model.)

3. Observations

The NATRE field experiment was performed in an open ocean region 1200 km west of the Canary Islands. The main experiment involved the controlled release in May 1992 of the passive tracer sulfur hexafluoride (SF_6) along a target density surface within the main pycnocline [*Ledwell et al.*, 1993; this issue]. The subsequent tracer concentration was observed over a series of sampling cruises, with the primary objectives of estimating the diapycnal diffusivity across the main pycnocline and studying lateral mixing and stirring on scales from 10 to 1000 km in the open ocean. The latter is the focus of the present study. In conjunction with the tracer, 10 neutrally buoyant Sound Fixing and Ranging (SOFAR) floats were also released to help track the tracer and to characterize the large-scale velocity field. The floats were preprogrammed to spend the majority of their time at nearly the same depth as the tracer, and were tracked for up to 1 year following deployment, thus allowing simultaneous observation of a passive tracer and Lagrangian particles.

3.1. NATRE Tracer

The tracer injection performed in May 1992 consisted of a series of closely spaced streaks in an area approximately 400 ($\pm$100) km^2 in horizontal extent [*Ledwell et al.*, this issue]. The target surface had a potential density of $\sigma_{0.3} = 28.05$, correponding to a depth of approximately 310 m. Sampling of the tracer began immediately after its release and was conducted on five cruises spanning $2\frac{1}{2}$ years. Sampling was performed during the 2 weeks after release, 5 and 6 months later (October to November 1992), 1 year after release (April to May 1993), and $2\frac{1}{2}$ years after release (November 1995). A thorough analysis of the injection and subsequent dispersal of the tracer is given by *Ledwell et al.* [this issue], and we discuss some of their results here, as they relate closely to our numerical simulations in section 4.

The horizontal distribution of tracer observed during the first 6 months is shown in Figure 1. This series of "snapshots," as measured by the NATRE sampling cruises, provides a vivid image of mixing and stirring in the open ocean. Of notable interest is the streak-like character of the tracer distribution observed during the October and November 1992 surveys. There appeared

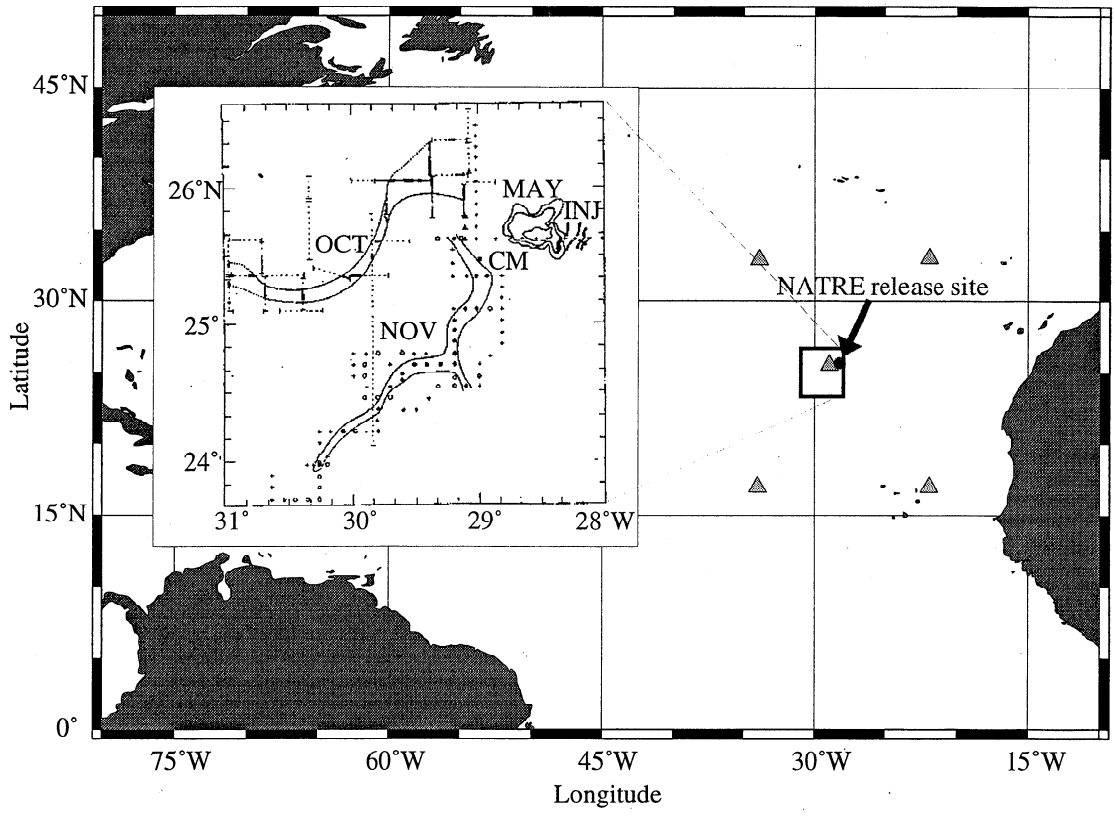

Figure 1. Horizontal distribution of tracer, expressed as the depth-integrated concentration, for the first 6 months of the North Atlantic Tracer Release Experiment (NATRE). The inset (reprinted by permission from *Nature* [*Ledwell et al.*, 1993] copyright 1993 Macmillan Magazines Ltd.) shows the location of the initial tracer injection streaks (marked INJ), contours of tracer 2 weeks after injection (marked MAY), and the two streaks observed in fall 1992 (marked OCT and NOV). The triangles are the locations of the five Subduction Experiment moorings.

to be two significant length scales that characterize the tracer distribution at this time. One was the radius of curvature of the streaks, which was set by the dominant length scale of the mesoscale eddies. The second was the rms width of the streaks, which was presumably set by a balance between the effective small-scale diffusion (on scales less than the streak width) and the mesoscale strain.

The ideas of section 1.1 may be applied to the NATRE observations in order to estimate an effective small-scale diffusivity κ_s. Assuming that after 6 months, the entire tracer patch was distributed in streaks similar to those observed, an exponential growth of streaks, $L = L_o e^{\lambda t}$, implied a streak growth rate of $\lambda \approx 3 \times 10^{-7}$ 1/s. Given the observed rms cross-streak width of $\sigma_{\rm rms} \approx 3$ km and using λ as a proxy for the rms strain rate (that is, $\gamma_{\rm rms} = \lambda$ exactly), the cross-streak balance between the strain rate and cross-streak diffusivity, $\kappa_s = \sigma_{\rm rms}^2 \lambda$, yielded an effective small-scale (less than 10 km) lateral diffusivity of $\kappa_s \approx 3$ m^2/s. As discussed by *Ledwell et al.* [1993, this issue], this value of κ_s can be compared with that predicted for shear dispersion by internal waves, $\kappa_s \approx 0.08$ m^2/s, that is presumed to act on scales of order 100 m [*Young et al.*, 1982]. The fortyfold discrepancy between these estimates of κ_s is intriguing and suggests that there was some horizontal mixing process acting at scales of order 1–10 km that was not anticipated by *Young et al.* [1982]. This result is based on the assumption that the exponential growth of tracer streaks and the approximate cross-streak balance between the convergent strain field and small-scale diffusion described by *Garrett* [1983] are valid in a fully turbulent flow. Numerical results discussed in section 4 support these assumptions.

Ledwell et al. [this issue] further reported that by May 1993 the tracer patch had become much more filled in comparison to the Fall 1992 surveys. Hence for the May 1993 and November 1994 surveys, they estimated a large-scale effective eddy diffusivity κ_e using the relation $2\kappa_e = \partial\sigma^2/\partial t$, where σ^2 now represents the large-scale variance of the tracer patch. From this, they obtained an effective eddy diffusivity of $\kappa_e \approx 1 \times 10^3$ m^2/s, a value consistent with estimates based on single-particle dispersion rates computed below from the NATRE float data. (The mean drift of the center of mass of the tracer patch was also estimated by *Ledwell et al.* [this issue] from the May 1993 tracer distribution. The mean westward component inferred from the tracer

data was consistent with flow estimates from hydrographic data, while the southward component inferred from the tracer was somewhat smaller. That there were only minor discrepancies between these Lagrangian and Eulerian estimates suggests that the movement of the center of mass of the tracer was primarily due to an Eulerian mean flow and not Lagrangian effects such as might arise from a large-scale gradient in eddy diffusivity [*Freeland et al.*, 1975].)

At this point, it is interesting to compare the qualitative nature of the NATRE tracer dispersal to the theoretical predictions of section 1.1 (Figure 2). For the exponential growth phase, consistent with *Ledwell et al.* [1993, this issue], we use a small-scale diffusivity $\kappa_s = 3$ m^2/s, and λ as a proxy for the rms strain rate, $\gamma_{\rm rms} = \lambda = 3 \times 10^{-7}$ 1/s. For the linear growth phase at large times, we assume, for simplicity, an isotropic large-scale eddy diffusivity $\kappa_e = 1 \times 10^3$ m^2/s (see above). To account for the finite size of the initial NATRE tracer patch, we plot the observations with a time offset of approximately 40 days, which corresponds to the time it would take for a point release of tracer to obtain an along-streak scale equal to that of the NATRE initial condition; that is, $2\sigma = (400 \text{ km}^2/\pi)^{1/2} = 11$ km.

Comparison of the patch area estimates of *Ledwell et al.* [this issue] with the theoretical predictions suggests that the lateral dispersal of the NATRE tracer was consistent with an exponential growth phase followed by a linear growth at large times. The correspondence of these two growth regimes with the observed streakiness and later homogenization of tracer is the most persuasive observational evidence in support of *Garrett*'s [1983] model.

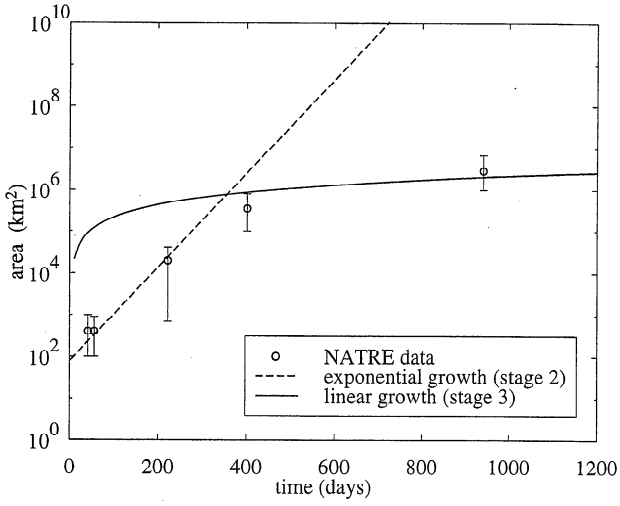

Figure 2. Exponential (dashed line) and linear (solid line) growth phases (stages 2 and 3 of section 1 in text) of tracer area for a theoretical point release of passive tracer in a turbulent flow and for the five sampling periods of NATRE (open circles). Theoretical curves are for effective diffusivity $\kappa_s = 3$ m^2 s, rms strain case $\gamma_{\rm rms} = 3 \times 10^{-7}$ 1/s, and effective eddy diffusivity $\kappa_e = 1 \times 10^3$ m^2/s. Patch area estimates for the NATRE data were taken from *Ledwell et al.* [this issue] and have been plotted with a time offset as described in text.

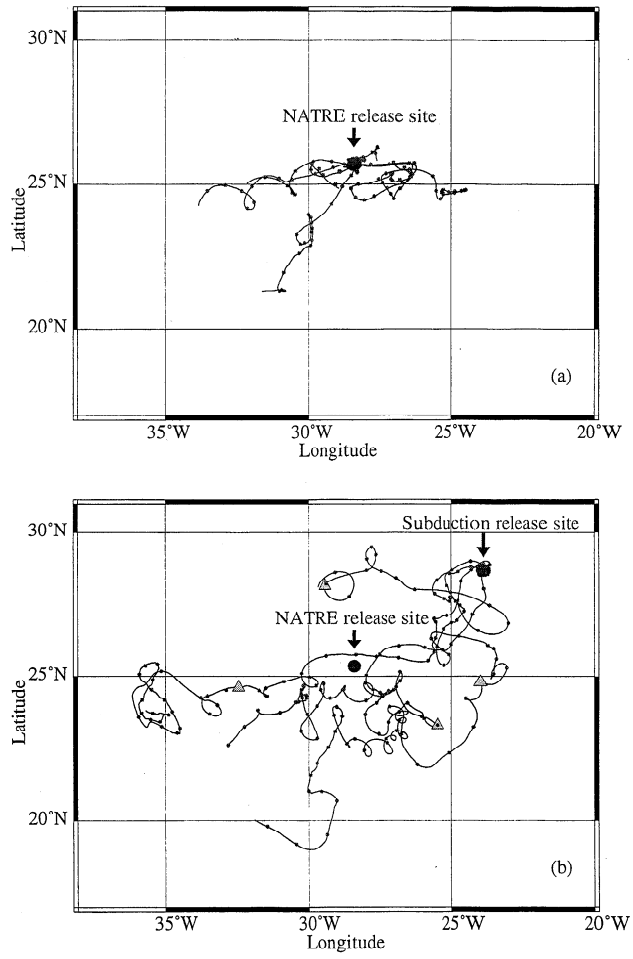

Figure 3. Float trajectories for (a) 1992–1993 NATRE floats (floats 55–64) and (b) 1991–1993 Subduction Experiment floats (floats 14,15,19,26). Triangles mark the locations of the four Subduction floats at the time of the NATRE release. Tick marks along trajectories correspond to 30-day intervals since release.

3.2. NATRE Floats

The 10 SOFAR floats released during NATRE were deployed along with the tracer in May 1992 and were tracked for up to 1 year after deployment, providing a total of about 57 float months of data (Figure 3). Each float was preprogrammed to make daily excursions through a portion of the water column while spending the majority of the day at a depth approximately equal to that of the tracer target density surface. The floats were tracked acoustically, with fixes of their positions given twice per day by an array of moored listening stations. Zonal and meridional velocity components were computed from the float positions using a cubic spline interpolation method.

All of the 10 NATRE floats provided reasonable velocity data during the time that they were transmitting, although two of the floats apparently experienced fail-

ure of either their pressure or temperature sensors. It is possible that these two floats settled to a deeper level than did the others; however, based on EKEs computed from individual float records, it does not seem that they were in a less energetic portion of the water column. We thus retain these data in our statistical analysis (in any case, the inclusion or exclusion of these data does not alter the main results of this study).

For the purpose of computing ensemble statistics, the 10 NATRE floats provided a somewhat limited sampling of the Lagrangian flow. Therefore, in the following analysis, we also incorporate data from four SOFAR floats of the Subduction Experiment that were deployed about 600 km northeast of the NATRE site in May 1991. The Subduction floats were of the same type as those used in NATRE except that they were equipped to transmit data for 2 years after deployment. The four floats of interest provided a total of 84 float months of data and were advected to the southwest through the site of the NATRE experiment, slightly above the target density surface between May 1991 and May 1993 (Figure 3). On the basis of expendable bathythermograph (XBT) profiles taken during the Subduction mooring deployment cruises [*Trask and Brink*, 1993], the average depths of these four Subduction floats were 285, 155, 170, and 170 m. Although three of these four floats were at shallower depths than the NATRE floats, we include them in our analysis in an attempt to obtain more robust statistics. It is possible that we thus bias our statistics (EKEs of each of the four Subduction floats were about 2 times larger than the NATRE floats); however, this should not affect the major results of this study, which depend on the comparison of numerical model results with theoretical predictions of tracer dispersal. A more detailed analysis of the combined float data set is given by *Sundermeyer* [1995].

Mean velocities computed from the full float data set are $(\overline{u}, \overline{v}) = (-1.2 \pm 0.3,\ -0.9 \pm 0.2)$ cm/s, while the zonal and meridional components of the combined time- and ensemble-averaged EKE are

$$\frac{1}{2}\overline{\langle u'^{2}_{(1,2)} \rangle} = (8.1 \pm 1.0,\ 8.0 \pm 0.9)\ \mathrm{cm}^2/\mathrm{s}^2.$$

Errors on means are given by the square root of the variance divided by the number of degrees of freedom, where the number of degrees of freedom is computed as the record length divided by twice the integral timescale ($[I_{11}, I_{22}] \approx [10.6, 5.4]$ days). The mean velocities computed from the float data are roughly in agreement with those estimated above from the tracer data, suggesting that the floats and tracer were advected similarly. (Ensemble means were computed under the assumption that each float represented an independent particle. This seems sensible, except for times shortly after release when floats are likely to be within the same flow features and behave in a spatially coherent fashion. Thus we may have slightly (by less than about 30%) overestimated the number of degrees of freedom.)

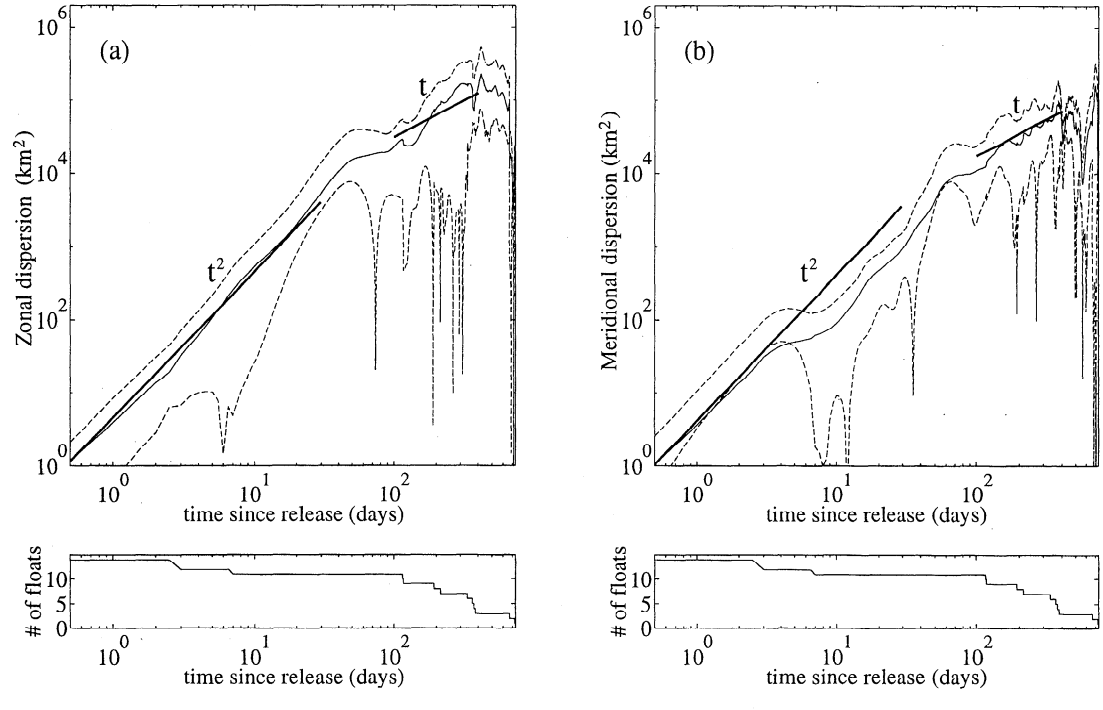

Figure 4. Time dependent (a) zonal and (b) meridional ensemble-averaged single-particle dispersions, $\langle x_i'^2(t) \rangle$, computed from NATRE and Subduction Experiment floats showing t^2 and t growth rates for short and long times, respectively. Solid lines are dispersion curves, while dashed lines indicate the uncertainty. Bold solid lines indicate t^2 and t growth rates. Number of floats as a function of time that made up the ensemble averages is shown at bottom.

The ensemble-averaged particle dispersion, $\langle x_i'^2(t)\rangle$, is plotted in Figure 4. In the limits of small and large t, the curves are roughly consistent with the predicted t^2 and t growth rates, respectively. For small times, (14) implies that on a log-log plot of dispersion versus time, the EKE should be given by the height of the dispersion curves (that is, it is proportional to the slope of these curves for small times). Figure 4 thus suggests EKE values of

$$\frac{1}{2}\overline{\langle u'^2_{(1,2)}\rangle} = (2.6 \pm 3.0, 2.4 \pm 4.7)\ \mathrm{cm^2/s^2},$$

where the uncertainty is computed as the square root of the variance divided by the number of independent pieces of data. The fact that values of EKE are somewhat lower than those made from the full record may reflect a bias at small t; that is, the floats may have been released into a flow feature that was less energetic than the average flow. Since the above direct estimates of EKE utilize the full data record and hence limit such bias by incorporating a larger number of degrees of freedom, we use those to compute the eddy diffusivities herein.

For long times, (16) suggests that the diffusivities $\kappa_{e_{ii}}$ can be estimated by the slope of the dispersion curves. A weighted least squares fit (on a linear-linear scale) between $t = 100$ and $t = 400$ days, where the dispersion at time t is weighted by the variance in the mean σ_i^2, yields $\kappa_{e_{(11,22)}} = (5.9 \pm 2.3,\ 1.9 \pm 0.7) \times 10^3\ \mathrm{m^2/s}$. These estimates of κ_e are approximately 2–6 times larger than those estimated above from tracer distributions in spring 1993 and fall 1994. This discrepancy may be a result of the small number of independent float observations used in the calculation. We suspect this because estimates of κ_e based on the product of the integral timescale and EKE (see below) give closer agreement with values estimated from tracer distributions.

Spatial and Lagrangian autocorrelation functions were computed from the float data according to the definitions given in section 2.2 (Figure 5). The first zero crossing of the transverse correlation function occurs at approximately 70 km, which is, not surprisingly, roughly comparable to the diameter of the loops formed by the float trajectories in Figure 3. Comparing the zonal and meridional LACFs, a slight anisotropy is apparent, with the meridional autocorrelation function showing a small negative lobe after its first zero crossing. Some degree of anisotropy was also evident in the tracer distributions [*Ledwell et al.*, this issue]. The first zero crossings of the LACFs occur between approximately 20 and 35 days, while it appears that the integrals of the LACFs are probably saturated after lags of about 40 days for the zonal correlation function and 60–70 days for the meridional correlation function. The locations of the changes in slope of the dispersion curves in Figure 4 imply similar saturation times of approximately 50 days for the zonal correlation function and 60–70 days for the meridional correlation function. Integrating the LACFs using 100 days as the upper limit of the integral of $R_{ii}(\tau)$ in (12) gives the integral timescales $I_{(11,22)} = (10.6 \pm 4.8,\ 5.4 \pm 2.8)$ days for the (zonal, meridional) components, where uncertainties represent 95% confidence limits estimated using a bootstrap method [e.g., *Press et al.*, 1986].

From these integral timescales and the combined time- and ensemble-averaged EKE, a second estimate of the zonal and meridional diffusivities yields $\kappa_{e_{(11,22)}} = (1.5 \pm 0.7,\ 0.7 \pm 0.4) \times 10^3\ \mathrm{m^2/s}$, where error estimates are based on the uncertainties of EKE and I_{ii} computed above. These estimates of κ_e are in close agreement

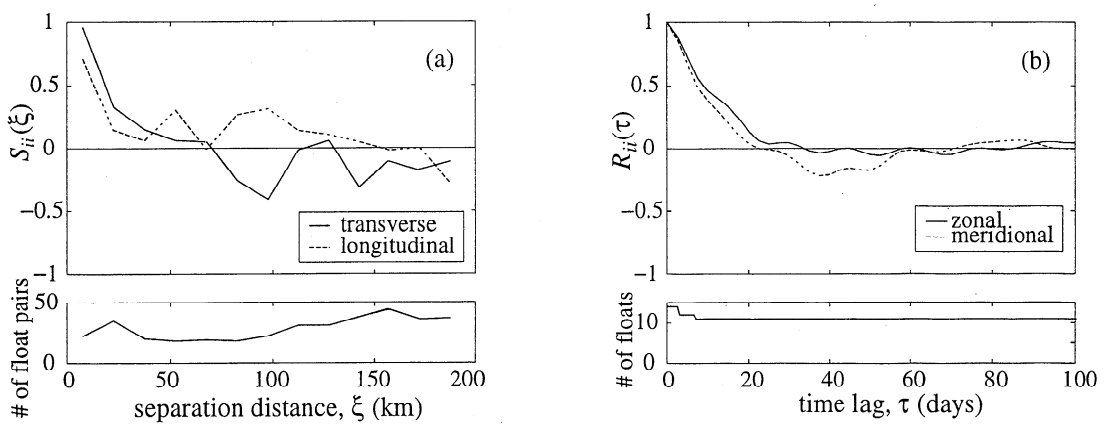

Figure 5. (a) Transverse (solid line) and longitudinal (dashed line) spatial correlation functions computed from NATRE and Subduction Experiment floats along with the number of float pairs used for a given separation distance. The covariances were averaged over 15 km bins of separation distance. (b) Zonal (solid line) and meridional (dashed line) ensemble-averaged Lagrangian autocorrelation functions computed from NATRE and Subduction Experiment floats along with the number of floats used for a given time lag.

with those computed by *Ledwell et al.* [this issue] from the tracer data.

4. Numerical Simulations

The results of the NATRE field experiment suggest that the theoretical ideas of *Garrett* [1983] and *Taylor* [1921] are relevant to the analysis of mesoscale stirring in the ocean. However, the NATRE tracer observations alone do not provide a means of quantitatively testing Garrett's theory, since we have no independent information about the strain and small-scale diffusivity. To address this, we now turn to numerical simulations of tracer dispersal in the presence of small-scale diffusion and a turbulent mesoscale strain field, where we do have knowledge of these quantities. A two-layer quasi-geostrophic vorticity model is calibrated so that the statistics of model floats agree as closely as possible with the NATRE floats. The main goal is to understand the possible biases and uncertainties associated with estimates of strain rate and small-scale diffusivity from the NATRE observations.

4.1. Model

We used a pseudo-spectral model (described by *Flierl et al.* [1987]) with two active layers and a mean vorticity gradient in the y coordinate direction. The model solves

$$\frac{\partial q_i}{\partial t} + J(\psi_i, q_i) = -\mu\nabla^2\psi_i + \nu\nabla^4\psi_i \qquad i = 1,2 \quad (17)$$

[e.g., *Pedlosky*, 1979], where the Jacobian operator $J(a,b) = \partial a/\partial x\ \partial b/\partial y - \partial a/\partial y\ \partial b/\partial x$, and μ and ν terms represent bottom friction (lower layer only) and Newtonian viscosity, respectively. The quasi-geostrophic potential vorticity q_i is given by

$$q_i = \nabla^2\psi_i - F_i(\psi_i - \psi_j) + f_o + \beta_i y, \qquad j = 3 - i, \quad (18)$$

where ψ_i is the geostrophic stream function for the ith layer, which satisfies

$$(u_i, v_i) = \hat{k} \times \nabla\psi_i = \left(\frac{-\partial\psi_i}{\partial y}, \frac{\partial\psi_i}{\partial x}\right), \quad (19)$$

$F_i = f_o^2/g'D_i$ is the inverse deformation radius squared, $g' = g\Delta\rho/\rho$ is the reduced gravity, and $(f_o + \beta y)$ is the planetary vorticity.

Forcing was achieved by imposing a westward mean flow $\overline{u_1}$ in the upper layer to serve as a source for baroclinic instability. A corresponding energy sink was provided by Newtonian viscosity in both layers plus bottom friction in the lower layer. (Additional simulations not discussed here were also run for a barotropic fluid using different forcing and dissipation mechanisms than described above. In particular, a random Markovian formulation was used to force the perturbation stream function across a narrow wavenumber band (160- to 210-km scales; e.g., *Maltrud and Vallis* [1991]), and an inverse Laplacian was used to dissipate energy at the largest scales [e.g., *Babiano et al.*, 1987]. These simulations can be compared with those of *Haidvogel and Keffer* [1984], the primary difference being the form of the forcing and dissipation mechanisms used to maintain the flow. We found that this barotropic model had to be rather heavily forced in order to achieve realistic time and space scales [*Sundermeyer*, 1995]. However, insofar as the tracer analysis went, no apparent differences were found between the barotropic and the present baroclinic simulations once a calibration had been achieved.) This configuration is identical to that used by *Haidvogel and Held* [1981], except that they used a biharmonic diffusion to dissipate enstrophy at small scales while we use an exponential filter at high wavenumbers [*Canuto et al.*, 1988]. An overview of the dynamics of two-dimensional vorticity models was given by *Rhines* [1977]. A more recent discussion of vortex dynamics in two-dimensional turbulence was given by *McWilliams* [1990].

Having computed the stream function in both layers from (17), the upper layer stream function is used to compute the evolution of a passive tracer field via the

Table 1. Parameter Settings Used in the Numerical Simulations

Parameter	Symbol	Nondimensional Value	Dimensional Value
Domain size		$2\pi \times 2\pi$	628 km × 628 km
Number of grid points		512	512
Grid spacing	Δx	0.012	1.2 km
Time step	Δt	0.0005	0.35 hour
Spin-up time		12.42	1.0 year
Run time		6.21	0.5 year
Baroclinic deformation radius	$1/\sqrt{F_1 + F_2}$	0.25	25 km
Aspect ratio	F_2/F_1	0.33	0.33
Planetary vorticity gradient	β	5.19	2.07×10^{-8} km/s
Newtonian viscosity	ν	7.5×10^{-4}	3.0 m^2/s
Bottom friction (layer 2 only)	μ	0.23	9.2×10^{-8} 1/s
Tracer diffusivity	κ_s	2.5×10^{-3}	10 m^2 1/s
Mean flow (layer 1 only)	$\overline{u_1}$	−0.78	−3.1 cm/s

advection/diffusion equation

$$\frac{\partial \theta}{\partial t} + J(\psi_1, \theta) = \kappa_s \nabla^2 \theta, \tag{20}$$

where κ_s is the explicit small-scale diffusivity. The motion of Lagrangian particles in the upper layer is computed using only the left-hand side of (20). Particles that are advected across the periodic boundaries are tracked as having done so, hence the total excursion of model floats may be larger than the model domain size.

The model was run on a square domain, with doubly periodic boundaries and 512 grid points in each horizontal direction. Redimensionalization was done by relating model EKE and planetary β to values appropriate to the NATRE experiment. Having set these two parameters, the following characteristic velocity, space, and time scales are obtained:

$$U = 4 \text{ cm/s} \tag{21}$$

$$L = 100 \text{ km} \tag{22}$$

$$T = 2.5 \times 10^6 \text{ s} \approx 29 \text{ days}. \tag{23}$$

This nonlinear system can be characterized by an advective timescale, $T \sim L/U$, so that once U is chosen, L and T are no longer independent. Other values of model parameters are given in Table 1.

4.2. Model Spin-up and Calibration

The flow was spun up for 1 year from an initial condition in which the perturbation stream functions were set to zero in the lower layer and assigned a random phase and an amplitude in the upper layer such that its energy spectrum was similar to the expected equilibrium spectrum. Model calibration was achieved by adjusting the relative strengths of the imposed mean flow $\overline{u_1}$ (note that this was the only forcing in the model) and the bottom friction μ, the objective being to achieve an upper layer flow that was similar in a statistical sense to that of the NATRE region. Three diagnostics were used to determine this: the eddy kinetic energy, the spatial correlation function, and the Lagrangian autocorrelation function. In all cases, model float statistics were computed in the same way as for the NATRE floats (see below). Parameter settings for a typical model solution that meets these calibration criteria are listed in Table 1.

An ensemble of 10 tracer simulations was run by reinitializing the model tracer every 6 months during a total simulation period of 5 years (not including spin-up). Figure 6 shows typical energy wavenumber spectra for the fully spun-up upper and lower layer along with a time series of the energy balance of the system. The k^{-5} dependence of spectra at high wavenumbers is similar to that found by *Haidvogel and Keffer* [1984] and is notably steeper than the k^{-3} slope predicted from simple energy and enstrophy conservation arguments for two-dimensional turbulence. Several investigators [e.g., *Basdevant et al.*, 1981; *Bennett and Haidvogel*, 1983; *Babiano et al.*, 1985; *Maltrud and Vallis*, 1991] have shown that steep spectral slopes may result from space-time intermittence and coherent structures of two-dimensional turbulence.

Floats were released into the upper layer, in a closely spaced array of 37 floats (intended to track the tracer; see Figure 7), superimposed on a uniformly spaced array of 100 floats that spanned the model domain (in order to insure robust statistics). For this example, mean velocities computed from the full array of floats were $u_{(1,2)} = (-3.2 \pm 1.6,\ 0.1 \pm 1.3)$ cm/s for the (eastward, northward) components and were, of course, consistent with our specified value of $\overline{u_1}$. The time- and ensemble-averaged EKEs were $(6.4 \pm 5.0,\ 7.0 \pm 4.8)$ cm^2/s^2 for the (eastward, northward) components and were within 20% of the EKE computed from the NATRE floats. The model SCFs (Figure 8) are similar to the SCFs com-

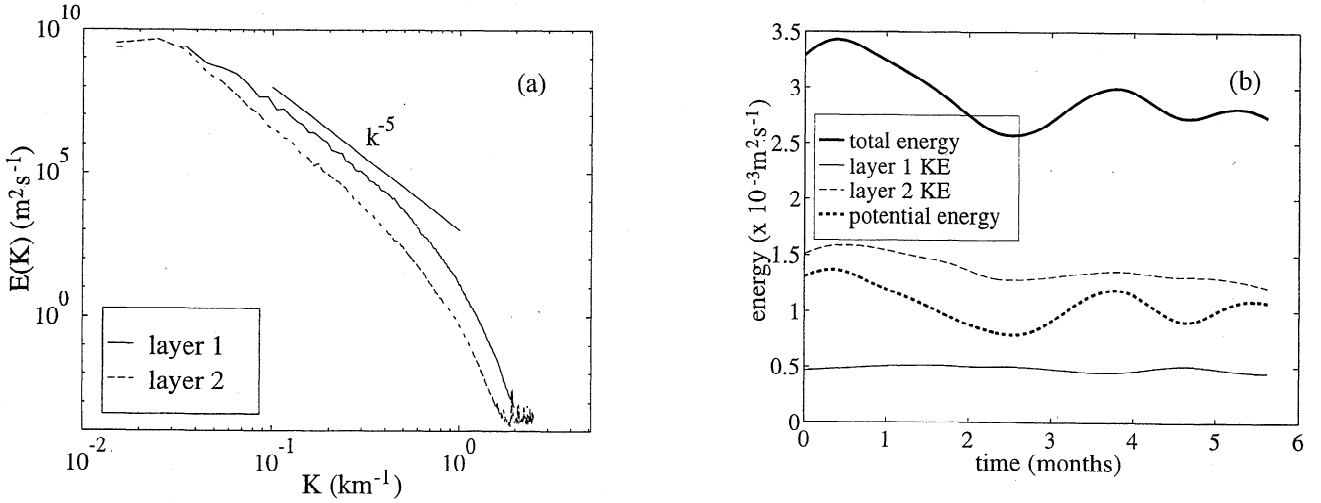

Figure 6. (a) Model energy spectra for upper and lower layer of a typical model run and (b) total (domain averaged) Eulerian energy budget for a typical 6-month integration.

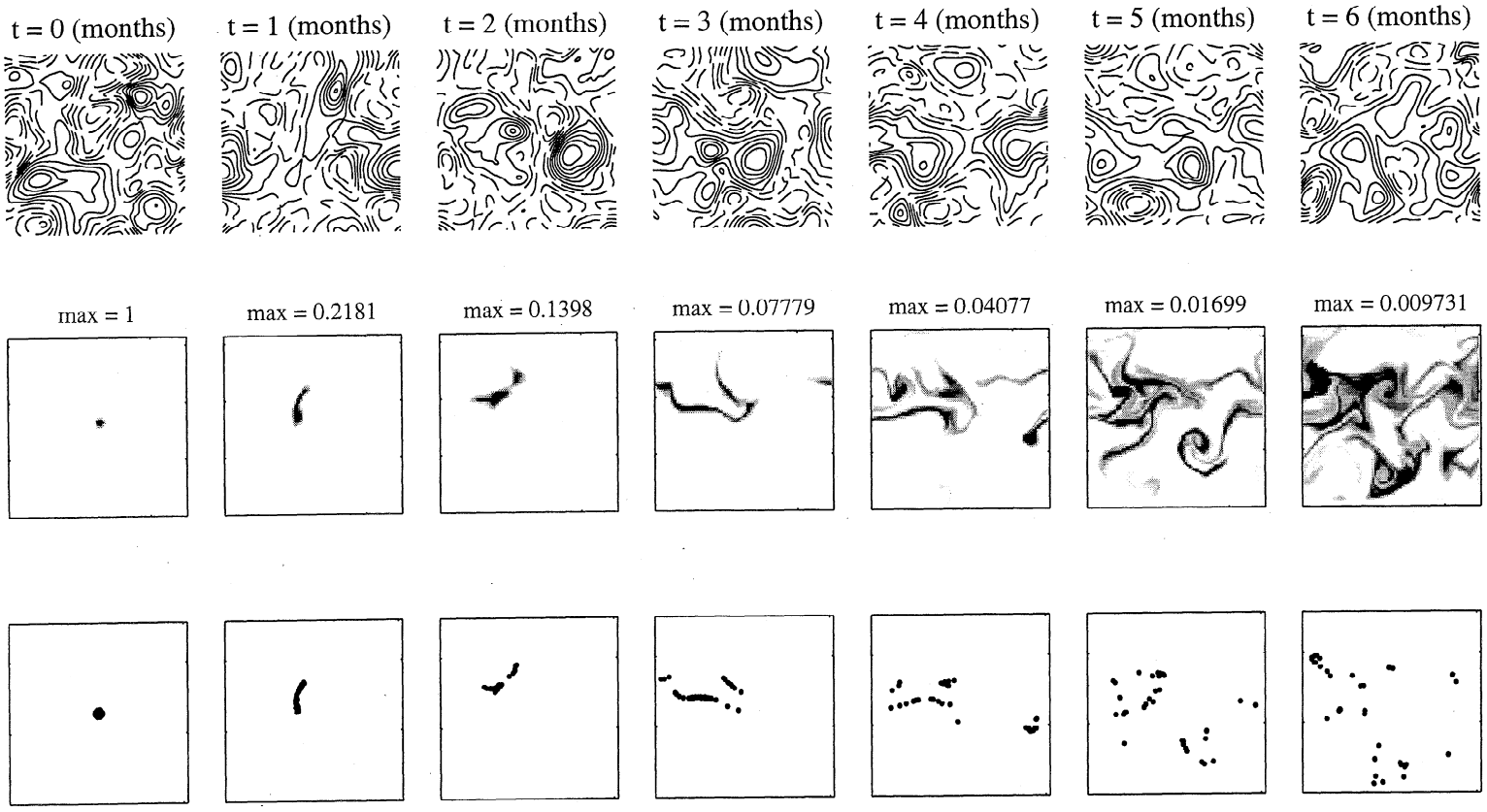

Figure 7. Perturbation stream function, tracer, and float positions (only those released within the patch; see text) for a typical model run. Successive frames (left to right) correspond to intervals of 1 month, with each frame representing an area of 628×628 km^2. Tracer maps are drawn with shading relative to the instantaneous maximum concentration, so that the concentration corresponding to the darkest shading decreases with time. Note the initial period of rapid streak formation followed by a more gradual "filling in" of tracer.

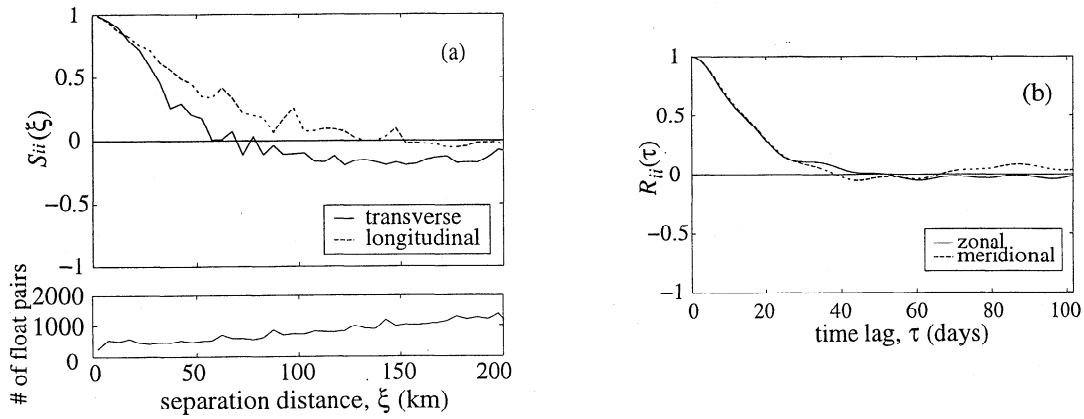

Figure 8. (a) Transverse (solid line) and longitudinal (dashed line) spatial correlation functions computed from model floats along with the number of float pairs used for a given separation distance. The calculated covariances were averaged over 5-km bins. (b) Ensemble-averaged zonal (solid line) and meridional (dashed line) Lagrangian autocorrelation functions computed from model floats. The number of floats used for a given time lag was 137.

puted from the NATRE floats (see Figure 5), with the transverse SCF having a first zero crossing at 70 km. Model zonal and meridional LACFs (Figure 8) both have their first zero crossings at approximately 28 days, which is also consistent with LACFs computed in section 3 from the NATRE observations. Given these results, we consider this solution to be calibrated.

4.3. Simulated Tracer Fields

A tracer was released into the fully spun-up upper layer. The initial tracer distribution was a Gaussian patch

$$\theta(x, y, t_o) = e^{-(x^2+y^2)/2\sigma^2} \tag{24}$$

of radius $2\sigma = 12.5$ km, intended as an idealization of the NATRE initial tracer distribution. The small-scale diffusivity in the model was set to 10 m^2/s or about 3 times larger than that inferred from the NATRE tracer observations. This was done to insure that tracer streaks were well resolved in the model, even in the presence of large strain rates. (Numerical experiments using a steady linear strain field, $\psi = -\gamma xy$ [not shown], were able to reproduce *Garrett*'s [1983] result, $\sigma^2_{\rm rms} = \kappa_s/\gamma_{\rm rms}$, provided that the streaks were well resolved, i.e., that they were always greater than about 8–10 grid points in width. For poorly resolved streaks, say 5 grid points wide, the observed streak width was about 50% greater than predicted by the relevant steady theory, presumably because of numerical diffusion.)

The evolution of the tracer field for a representative model solution is shown in Figure 7. By comparing the floats and tracer, it can be seen that the two are advected together, as expected. Qualitatively, the dispersal of model tracer appears consistent with both theoretical expectations and observations from NATRE. Immediately after release, there is a period of rapid streak formation, characterized by a fairly well defined streak width. For longer times, the streaks begin to wrap around one another and merge, gradually filling in the model domain. The tracer concentration and area are not considered for times greater than about 6 months, at which time the tracer has wrapped around the model domain.

We now mimic the analysis of the NATRE tracer (section 3.1), assuming no a priori information about the flow, and attempt to infer the small-scale diffusivity via estimates of streak width and strain rate. Using $T = 3$ months from our representative model solution (streak length in this simulation becomes ambiguous after this time; see frames of $t = 4$ to $t = 6$ months in Figure 7), we estimate a streak length of approximately 800 km or $L = 2\sigma \approx 400$ km, which would imply a streak growth rate of $\lambda \approx 4.5 \times 10^{-7}$ 1/s. Using λ as a proxy for the rms strain rate (i.e., taking $\gamma_{\rm rms} = \lambda$ exactly) and using a value for the rms cross-streak variance $\sigma^2_{\rm rms} \approx 28$ km^2 estimated from sections of the tracer (Figure 9), the assumed balance $\kappa_s = \sigma^2_{\rm rms}\gamma_{\rm rms}$ yields a small-scale diffusivity of $\kappa_s = 13$ m^2/s, which is about 30% larger than the explicit small-scale diffusivity set in the model. Repeating this analysis for the set of 10 simulations, we obtain, on average, $\kappa_s = 19.0 \pm 10.5$ m^2/s or approximately twice the explicit small-scale diffusivity set in the model (the uncertainty here is twice the sample standard deviation).

This is one of the most significant results of our numerical simulations. It shows that if λ is used as the strain rate in the expression for the cross-streak balance, then the predicted κ_s is biased by a factor of 2 but is otherwise fairly robust. An unbiased estimate obtains if we use $\sigma^2_{\rm rms} = \kappa_s/(\lambda/2)$. This suggests that the more than order of magnitude discrepancy between κ_s estimated by *Ledwell et al.* [this issue] and that predicted for shear dispersion by *Young et al.* [1982] is very reliable. (K. L. Polzin et al., manuscript in preparation,

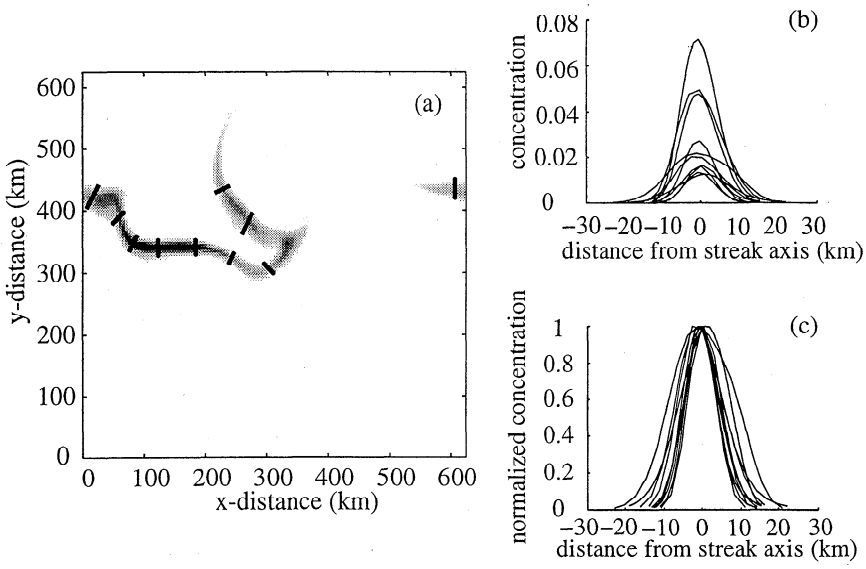

Figure 9. Cross-streak profiles of model tracer mimicking those obtained during the October and November NATRE cruises showing a "well-defined" rms streak width. (a) Model tracer distribution is the same as $t = 3$ months in Figure 7, corresponding to approximately 3 months since release. Solid lines represent the locations of tracer sampling sections. (b) Absolute and (c) normalized concentrations along the sections, plotted with the streak axis centered at zero.

1998) have suggested that shear dispersion associated with the vortical mode, which is not accounted for in the theory of *Young et al.* [1982], may be responsible for this discrepancy. However, further investigation of this process is beyond the scope of this study.)

Next, we compare qualitatively the growth of the model tracer area with that predicted from theory.

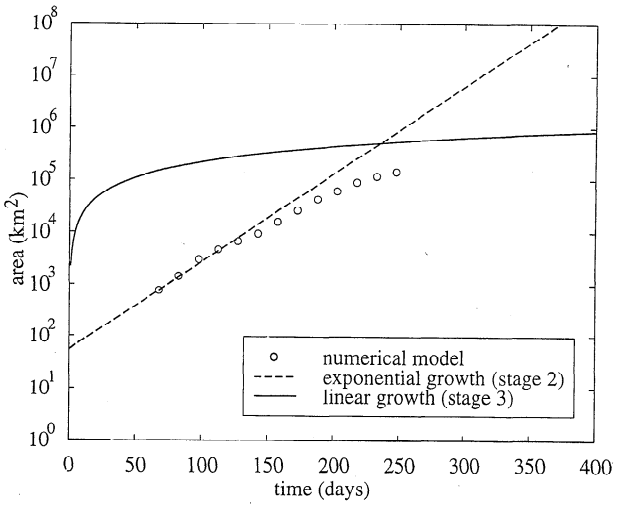

Figure 10. Exponential (dashed line) and linear (solid line) growth phases (stages 2 and 3 of section 1 in text) of tracer area for a theoretical point release of passive tracer in a turbulent flow and model results (open circles) for Figure 7. Theoretical curves are for $\kappa_s = 10.0\ \mathrm{m^2/s}$, $\gamma_{\mathrm{rms}} = 4.5\times10^{-7}\ 1/\mathrm{s}$, and $\kappa_e = 1\times10^3\ \mathrm{m^2/s}$. Model results are plotted with a time offset of approximately 70 days to compensate for the finite size of the initial release.

For the small-scale diffusivity, we use the model value $\kappa_s = 10\ \mathrm{m^2/s}$, while for the rms strain rate, we again use the streak growth rate $\lambda = 4.5 \times 10^{-7}\ 1/\mathrm{s}$, estimated above. For the large-scale effective eddy diffusivity, we use $\kappa_e = 1 \times 10^3\ \mathrm{m^2/s}$, consistent with estimates from NATRE. The area of the tracer patch of our representative solution, computed as the area within the highest contour bounding 95% of the tracer, is plotted along with the corresponding theoretical curves in Figure 10. As with the NATRE observations, there is a clear exponential growth phase followed by a reduced growth rate, perhaps approaching a linear regime, at long times (the linear growth phase for long times is not sampled adequately here owing to limitations in model domain size).

Pertinent to the above calculations, the clear exponential growth seen in Figure 10 associated with rapid streak formation is the most compelling argument for using *Garrett*'s [1983] scaling results to estimate the effective small-scale diffusivity. As noted above, this period is characterized by a fairly well defined streak width that permits unambiguous (although perhaps biased) estimates of κ_s.

5. Discussion

The above analysis suggests that the predictions of section 1.1 can be calibrated with numerical simulations and used to make unbiased estimates of κ_s based on observations from a tracer release experiment. If λ is used as a proxy for the rms strain rate, an unbiased estimate of κ_s obtains for $\sigma^2_{\mathrm{rms}} = \kappa_s/(\lambda/2)$. For practical purposes, this is a very useful result, and, in principle,

we could stop here. However, there are some interesting questions that merit further consideration. How are the different measures of the strain rate related to one another? Is the calibration factor in the above result sensitive to spatial and temporal variations of the strain rate and streak width? Could a bias also occur if we overestimate the mean streak width as a result of the merging of tracer streaks? We now address these questions in turn.

5.1. Streak Growth Rates and Strain Rates

To understand the relationship between the streak growth rate and the strain rate, consider our expression (9) for streak length in a time dependent but spatially constant strain field. In that case, the mean strain rate may be defined as $\langle\gamma\rangle = \frac{1}{t}\int_0^{t'} \gamma(t)dt$ and is equal to the streak growth rate; that is, $\lambda = \alpha\langle\gamma\rangle$, with $\alpha = 1$. As pointed out by *Garrett* [1983], however, this equality depends on what one uses as a measure of the strain rate. For example, he used $\gamma_{\rm rms} = \langle(\partial u/\partial x)^2 + (\partial v/\partial y)^2\rangle^{1/2}$, which for the time dependent problem would imply an exponential growth coefficient $\alpha = 1/\sqrt{2}$. Yet another measure of the strain rate, suggested by *Haidvogel and Keffer* [1984], is given by the diagonalized strain tensor, $\gamma_{\rm rms} = \langle -\partial u/\partial x\ \partial v/\partial y + 1/4\,(\partial u/\partial y + \partial v/\partial x)^2\rangle^{1/2}$, which would require still another value for α.

In the general case of a temporally and spatially varying strain field, it is not immediately clear which, if any, of the above strain rates is the best estimator of the strain rate needed to evaluate κ_s. Intuitively, we might expect some average of the along-streak component of the strain rate γ_s to be most appropriate and most nearly equal to the mean streak growth rate. Some evidence for this can be found in our numerical results if we compare the along-streak component of the strain rate γ_s computed directly from the model stream function to the streak growth rate λ estimated from the model tracer fields. Averaging over the area strained by the tracer (the area within the highest contour encompassing 95% of the tracer) for $t = 3$ months of our representative model, we find $\langle\gamma_s\rangle = 2.8\times10^{-7}\pm7.1\times10^{-9}$ 1/s, where the uncertainty is given by the standard error (Figure 11). This is about 60% smaller than the average streak growth rate estimated directly from the tracer, i.e., for this definition of the strain rate, $\lambda \approx 2\langle\gamma_s\rangle$. *Ledwell et al.* [this issue] suggest that the mean streak growth rate may be weighted by the largest strains along the streak and should be larger than the averaged along-streak strain rate.

If we similarly compute the averaged strain rate as defined by the diagonalized strain tensor, we find values that are 3 to 6 times larger than the streak growth rate. Thus, while the averaged along-streak component of the strain rate is somewhat smaller than the streak growth rate, the diagonalized strain tensor is many times larger. A similar result was reported by *Pope* [1990] for simulations of three-dimensional turbulence, namely, his mean "maximum extensive strain" was 3 times the "mean strain rate on a material line." From this, we conclude that for estimating the small-scale diffusivity from *Garrett*'s [1983] theory, the along-streak component of the strain rate is a more appropriate measure of the strain rate than the diagonalized strain tensor.

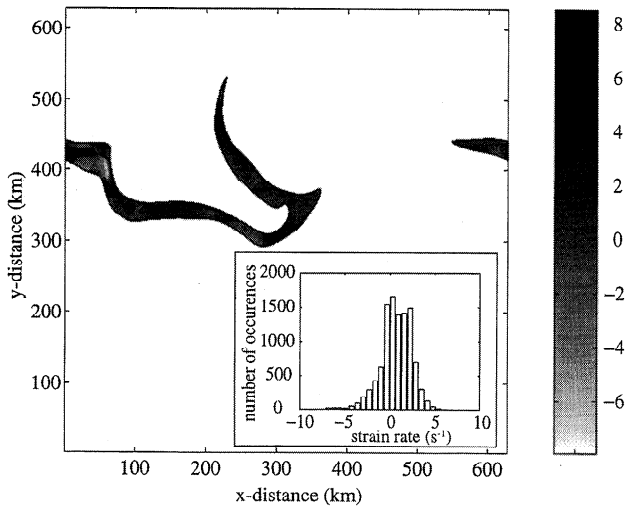

Figure 11. Along-streak component of model strain rate computed within the 95% contour of tracer (solid line) for $t = 3$ of Figure 7. The rms strain rate is $\langle\gamma_s\rangle = 2.8\times10^{-7}\pm7.2\times10^{-7}$ 1/s; the inset shows a histogram of the strain rates computed at each model grid point.

5.2. Temporal and Spatial Variations

Locally, along some segment of a tracer streak, we expect that a balance obtains between some (possibly weighted) average of the directional strain rate and the small-scale diffusivity; that is, $\sigma^2_{\rm rms} = \kappa_s/\langle\gamma_s\rangle$. However, the directional strain rate (and, in fact, any of the above measures of the strain rate) varies significantly on scales that are small compared with the streak width, which violates the assumption that the strain rate is uniform within a given streak (Figure 11). In fact, a histogram of the directional strain rates (inset in Figure 11), shows both negative as well as positive values of γ_s; that is, the flow is not even always divergent in the along-streak direction. At first, this may seem counterintuitive; after all, it is the sign of the divergence that should determine the along- and cross-streak direction of the tracer. However, such changes in the direction of the strain rate on scales smaller than the streak width are consistent with the splitting and bifurcating of tracer streaks seen in both the observations and the numerical solutions (Figures 1 and 7).

How these small-scale spatial variations in the strain rate affect estimates of κ_s is unclear. Even if we could construct some appropriate spatial average, we must still contend with the mixed temporal variations in the strain rate (see also *Pope* [1990] for a discussion of temporal variations in strain in three-dimesional turbulence). This is illustrated by (8), which shows that the covariance between the strain rate and the cross-

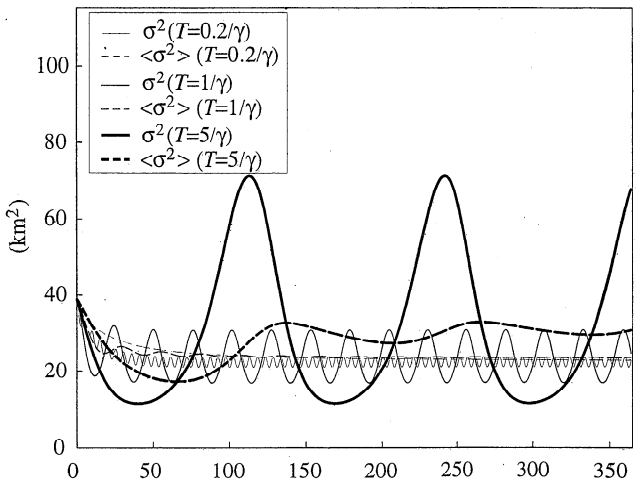

Figure 12. Theoretical solution for a sinusoidally varying strain rate showing a mean cross-streak variance that is biased high when the strain rate varies slowly in time. Solid lines represent the instantaneous cross-streak variances σ_y^2 for $\gamma(t)$ oscillating with periods $T = 0.2 \times 1/\gamma$, $T = 1/\gamma$, and $T = 5 \times 1/\gamma$. Dashed lines represent the running mean of the corresponding cross-streak variances $\langle \sigma_y^2 \rangle$.

streak variance may be important. For example, for a slowly varying strain rate (slow compared to the advective timescale, $1/\gamma$), the strain rate and streak width are approximately in balance and are negatively correlated. In that case, neglecting the covariance term would lead to an overestimate of κ_s, consistent with results from our numerical experiments.

Using (9) as a solution for the cross-streak variance σ_y (and letting $\gamma < 0$), we may also compare the case of a slowly varying strain rate to one that varies rapidly in time. Consider a time dependent strain rate of the form $\gamma = \gamma_o[1 + \sin(2\pi/T\ t)]$. For $T \ll 1/\gamma_o$, we find that the long-term mean $\langle \sigma_y^2 \rangle$ closely resembles the solution for a constant strain rate with $\gamma \equiv \gamma_o$ as does the same sinusoidal solution with $T \sim 1/\gamma_o$ (Figure 12). On the other hand, a slowly varying strain rate, $T \gg 1/\gamma_o$, leads to a mean $\langle \sigma_y^2 \rangle$ that is significantly greater than the steady solution. The reason for this can be seen by considering the form of the exponential growth rate in this case,

$$\Gamma = \int_0^{t'} \gamma(t)dt = \gamma_o\{t - \frac{1}{2\pi/T}[\cos\left(\frac{2\pi}{T}t\right) + 1]\}.$$

This shows that for $T \leq 1/\gamma_o$, for time $t \gg 1/\gamma_o$, Γ/t approaches γ_o, which is precisely the mean value of $\gamma(t)$.

This example suggests that rapid variations in $\gamma(t)$ do not significantly alter the long-term/steady balance between the streak width and the strain rate. However, slow variations in the strain rate may bias high our estimates of κ_s. Returning to our numerical results, it is interesting to assess in which regime our solutions lie. To determine this, we calculate directly the time dependent strain rate following a marked fluid parcel (Figure 13). This reveals that the along-streak component of the strain varies considerably on timescales greater than or equal to $1/\gamma$. We thus conclude that temporal variations in the strain rate may account for as much as 30% of the bias in our estimate of κ_s. (Whether this estimate is affected by small-scale spatial variations is unclear.)

5.3. Merging of Tracer Streaks

A third and final possible bias in our estimates of small-scale diffusivity stems from the merging of tracer streaks which must occur in order for the tracer to fill in the patch (see Figure 7). When two streaks merge, each effectively loses its identity, leaving a single streak that is initially wider than either of the component streaks. From an observer's perspective, the inability to distinguish individual streaks from those that have resulted from a recent merger could lead to an overestimate of the streak width, which would lead, in turn, to the overestimation of κ_s. We were careful to avoid this bias in our analysis of simulated tracer, but, of course, we had nearly complete information about the model tracer. This may not always be possible in real oceanic tracer release experiments. However, the careful planning and execution of sampling surveys combined with an understanding of the time and space scales of the mesoscale flow should help avoid this bias.

6. Summary and Conclusions

In this study we have shown that the dispersal of a passive tracer in NATRE can be described using the ideas laid out by *Garrett* [1983] and that such tracer experiments can be simulated realistically using an appropriately calibrated numerical model.

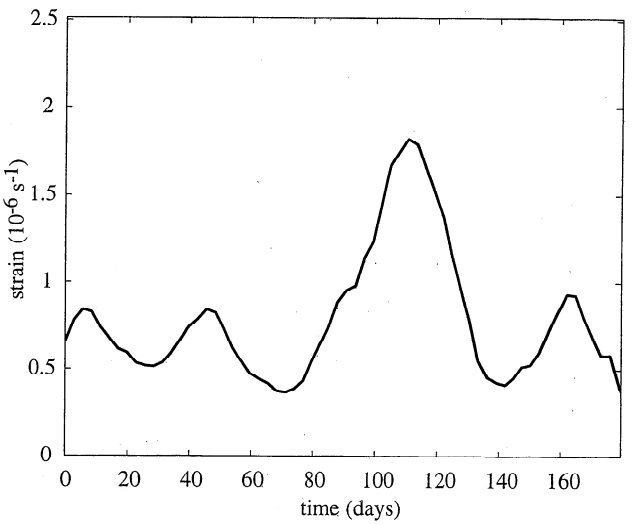

Figure 13. Along-streak component of the model strain rate following a Lagrangian particle. Order 1 fluctuations are readily apparent on timescales that are long compared with $1/\gamma \approx 26$ days, suggesting that the strain rate and streak width are likely to be negatively correlated.

The streakiness phase of the NATRE tracer patch was consistent with an exponential growth of tracer area for values of small-scale diffusivity, $\kappa_s = 3\ \mathrm{m}^2/\mathrm{s}$, and streak growth rate, $\lambda = 3 \times 10^{-7}$ 1/s, as previously estimated by *Ledwell et al.* [1993, this issue]. Large-scale effective eddy diffusivities computed from the NATRE float observations were $(\kappa_{e_{11}}, \kappa_{e_{22}}) = (1.5 \pm 0.7,\ 0.7 \pm 0.4) \times 10^3$ m^2/s for (zonal, meridional) components. These values agree with estimates based on the growth of the second moments of the tracer patch by *Ledwell et al.* [this issue] and describe the approximately linear growth of the patch area at long times.

Statistics computed from the NATRE float data were used to characterize the kinematics of the mesoscale flow. Mean velocities of $(\overline{u}, \overline{v}) = (-1.2 \pm 0.3,\ -0.9 \pm 0.2)$ cm/s estimated from the float data were roughly consistent with those estimated by *Ledwell et al.* [this issue] from movement of the tracer patch. The ensemble-averaged (zonal, meridional) EKEs were $(8.1 \pm 1.0,\ 8.0 \pm 0.9)$ $\mathrm{cm}^2/\mathrm{s}^2$. The first zero crossing of the transverse SCF occurred at approximately 70 km, while (zonal, meridional) integral timescales estimated from the integral of the LACFs were $I_{(11,22)} = (10.6 \pm 4.8,\ 5.4 \pm 2.8)$ days.

A two-layer, quasi-geostrophic vorticity model was used to simulate the stirring and mixing of a passive tracer in a turbulent flow. The model was calibrated so that the basic statistics of the model floats agreed as closely as possible with those computed from the NATRE floats (EKE and spatial and Lagrangian autocorrelation functions). The rate of dispersal of model tracer was then examined in order to assess the quantitative agreement between the theoretical model of *Garrett* [1983] and tracer dispersal in a fully turbulent flow. The dispersal of model tracer was found to be consistent with an exponential growth phase, followed by a reduced growth rate, perhaps approaching a linear regime for long times. Using the streak growth rate estimated directly from the tracer as a proxy for the rms strain rate in the formula of *Garrett* [1983] for the cross-streak balance (as must be done in any real tracer release study, since γ_{rms} cannot be measured directly), we found that a factor of 2 is required to obtain an unbiased estimate of the effective small-scale diffusivity κ_s (that is, κ_s is otherwise biased high by a factor of 2). An appropriate measure of the strain rate in Garrett's theory may be the averaged along-streak component of the strain rate, which we found was roughly half the streak growth rate computed directly from the tracer patch. The rms strain rate computed from the diagonalized strain tensor was 3 to 6 times larger than the streak growth rate, and is therefore less appropriate. A second possible source of bias in estimates of κ_s from tracer observations results from the temporal and spatial variations in the strain field, particularly the negative correlation between streak width and strain rate, which are necessarily neglected by *Garrett*'s [1983] theory.

These assessments of the spatial and temporal effects in our numerical experiments suggest that estimates of the effective small-scale diffusivity κ_s inferred from the NATRE tracer by *Ledwell et al.* [1993] may have been too large by about a factor of 2, and *Ledwell et al.* [this issue] have adjusted their estimates downward in light of these results.

A third potential source of bias brought to light by our numerical simulations is that as tracer streaks begin to merge, it may not be possible from local measurements to distinguish individual streaks from recently merged (and broader) streaks. Whether such a bias occurred in computations of κ_s from the NATRE field data is not known, but it is considered unlikely.

Given the agreement between the theoretical predictions of *Garrett* [1983] and our numerical results, we conclude that no known biases could account for the order of magnitude discrepancy between the effective small-scale diffusivity estimated from NATRE ($\kappa_s \approx 2$ to $3\ \mathrm{m}^2/\mathrm{s}$) and that predicted for shear dispersion by internal waves ($\kappa_s \approx 0.08\ \mathrm{m}^2/\mathrm{s}$). It is more likely that this discrepancy is due to the presence of some real but as yet unidentified horizontal mixing process acting on scales of 1–10 km.

Acknowledgments. Support for M.A.S. and J.F.P. was provided by the National Science Foundation under grant OCE90-05738. The original code for the numerical model was written by William K. Dewar and Glenn R. Flierl. Some additional code was provided by Audrey Rogerson and Joseph LaCasce. Sincerest thanks to James Ledwell, Andrew Watson, and Clifford Law for sharing their data and especially to James Ledwell for many stimulating discussions. Thanks also to John Toole and two anonymous reviewers for comments on the manuscript. This is contribution 9682 from the Woods Hole Oceanographic Institution.

References

Babiano, A., C. Basdevant, and R. Sadourny, Structure functions and dispersion laws in two-dimensional turbulence, *J. Atmos. Sci.*, *42*, 941–949, 1985.

Babiano, A., C. Basdevant, B. Legras, and R. Sadourny, Vorticity and passive-scalar dynamics in two-dimensional turbulence, *J. Fluid Mech.*, *183*, 379–397, 1987.

Basdevant, C., B. Legras, R. Sadourny, and M. Béland, A study of barotropic model flows: Intermittency, waves and predictability, *J. Atmos. Sci.*, *38*, 2305–2326, 1981.

Bennett, A. F., A Lagrangian analysis of turbulent diffusion, *Rev. Geophys.*, *25*, 799–822, 1987.

Bennett, A. F., and D. B. Haidvogel, Low-resolution numerical simulation of decaying two-dimensional turbulence, *J. Atmos. Sci.*, *40*, 738–748, 1983.

Canuto, C., M. Y. Hussaini, A. Quarteroni, and T. A. Zang, *Spectral Methods in Fluid Dynamics*, 557 pp., Springer-Verlag, New York, 1988.

Colin de Verdiere, A., Lagrangian eddy statistics from surface drifters in the eastern North Atlantic, *J. Mar. Res.*, *41*, 375–398, 1983.

Davis, R. E., Oceanic property transport, Lagrangian particle statistics, and their prediction, *J. Mar. Res.*, *41*, 163–194, 1983.

Davis, R. E., Drifter observations of coastal surface cur-

rents during CODE: The statistical and dynamical views, *J. Geophys. Res.*, *90*, 4756–4772, 1985.
Davis, R. E., Modeling eddy transport of passive tracers, *J. Mar. Res.*, *45*, 635–666, 1987.
Eckart, C., An analysis of the stirring and mixing processes in incompressible fluids, *J. Mar. Res.*, *7*, 265–275, 1948.
Fischer, H. B., E. J. List, R. C. Y. Koh, J. Imberger, and N. H. Brooks, *Mixing in Inland and Coastal Waters*, 483 pp., Academic, San Diego, Calif., 1979.
Flierl, G. R., P. Malanotte-Rizzoli, and N. J. Zabusky, Nonlinear waves and coherent vortex structures in barotropic β-plane jets, *J. Phys. Oceanogr.*, *17*, 1408–1438, 1987.
Freeland, H. J., P. B. Rhines, and T. Rossby, Statistical observations of the trajectories of neutrally buoyant floats in the North Atlantic, *J. Mar. Sci.*, *33*, 383–404, 1975.
Garrett, C., On the initial streakiness of a dispersing tracer in two- and three-dimensional turbulence, *Dyn. Atmos. Oceans*, *7*, 265–277, 1983.
Haidvogel, D. B., and I. M. Held, Homogeneous quasi-geostrophic turbulence driven by a uniform temperature gradient, *J. Atmos. Sci.*, *37*, 2644–2660, 1981.
Haidvogel, D. B., and T. Keffer, Tracer dispersal by mid-ocean mesoscale eddies, I, Ensemble statistics, *Dyn. Atmos. Oceans*, *8*, 1–40, 1984.
Holloway, G., and S. S. Kristmannsson, Stirring and transport of tracer fields by geostrophic turbulence, *J. Fluid Mech.*, *141*, 27–50, 1984.
Ledwell, J. R., A. J. Watson, and C. S. Law, Evidence for slow mixing across the pycnocline from an open-ocean tracer-release experiment, *Nature*, *364*, 701–703, 1993.
Ledwell, J. R., A. J. Watson, and C. S. Law, Mixing of a tracer released in the pycnocline, *J. Geophys. Res.*, this issue.
Maltrud, M. E., and G. K. Vallis, Energy spectra and coherent structures in forced two-dimensional and beta-plane turbulence, *J. Fluid Mech.*, *228*, 321–342, 1991.
McWilliams, J. C., The vortices of two-dimensional turbulence, *J. Fluid Mech.*, *219*, 361–385, 1990.
Pedlosky, J., *Geophysical Fluid Dynamics*, 710 pp., Springer-Verlag, New York, 1979.
Pope, S. B., Lagrangian microscales in turbulence, *Philos. Trans. R. Soc. London, Ser. A*, *333*, 309–319, 1990.
Press, W. H., S. A. Teukolsky, W. T. Vetterling, and B. P. Flannery, *Numerical Recipes*, 933 pp., Cambridge Univ. Press, New York, 1986.
Rhines, P. B. The dynamics of unsteady currents, in *The Sea*, vol. 6, edited by E. D. Goldberg et al., chap. 7, pp. 189–318, John Wiley, New York, 1977.
Sundermeyer, M. A., Mixing in the North Atlantic Tracer Release Experiment: Observations and numerical simulations of Lagrangian particles and passive tracer, M.S. thesis, 90 pp., Joint Program in Phys. Oceanogr., Mass. Inst. of Technol., Cambridge, Woods Hole Oceanogr. Inst., Woods Hole, Mass., 1995.
Taylor, G. I., Diffusion by continuous movements, *Proc. London Math. Soc. A*, *20*, 196–212, 1921.
Townsend, A. A., The diffusion of heat spots in isotropic turbulence, *Proc. R. Soc. London, Ser. A*, *209*, 418–430, 1951.
Trask, R. P., and N. J. Brink, Cruise report R/V Oceanus cruise # 240, leg 3. Subduction 1 Mooring Deployment Cruise, 17 June – 5 July, 1991, *Tech. Rep. 93-12*, Woods Hole Oceanogr. Inst., Woods Hole, Mass., 1993.
Young, W. R., P. B. Rhines, and C. J. R. Garrett, Shear-flow dispersion, internal waves and horizontal mixing in the ocean, *J. Phys. Oceanogr.*, *12*, 515–527, 1982.

J. F. Price, Department of Physical Oceanography, Woods Hole Oceanographic Institution, Clark 209A, Mail Stop 29, Woods Hole, MA 02543. (email: jprice@whoi.edu)

M. A. Sundermeyer, Center for Marine Science and Technology, University of Massachusetts, Dartmouth, 706 South Rodney French Boulevard, New Bedford, MA 02744. (email: msundermeyer@umassd.edu)

(Received October 20, 1997; revised April 30, 1998; accepted May 22, 1998.)